

The Celestial Reference Frame at X/Ka-band (8.4/32 GHz)

C. S. Jacobs, J. E. Clark, M. B. Heflin, L. J. Skjerve, O. J. Sovers
Jet Propulsion Laboratory, California Institute of Technology, 4800 Oak Grove Dr., Pasadena CA 91109, USA

C. Garcia-Miro, V. E. Moll
Ingenieria y Servicios Aeroespaciales, Instituto Nacional de Técnica Aeroespacial/NASA
Madrid Deep Space Communication Complex, Paseo del Pintor Rosales, 34 bajo, E-28008 Madrid, Spain

S. Horiuchi
C.S.I.R.O. Astronomy and Space Science/NASA, PO Box 1035, AU Tuggeranong ACT 2901, Australia

Abstract. A celestial reference frame at X/Ka-band (8.4/32 GHz) has been constructed using fifty-one 24-hour sessions with the Deep Space Network. We report on observations which have detected 436 sources covering the full 24 hours of right ascension and declinations down to -45 deg. Comparison of this X/Ka-band frame to the S/X-band (2.3/8.4 GHz) ICRF2 shows wRMS agreement of 200 micro-arcsec (μas) in $\alpha \cos \delta$ and 290 μas in δ . There is evidence for zonal errors at the 100 μas level. Known errors include limited SNR, lack of phase calibration, troposphere mismodelling, and limited southern geometry. The motivations for extending the ICRF to frequencies above 8 GHz are to access more compact source morphology for improved frame stability, to provide calibrators for phase referencing, and to support spacecraft navigation at Ka-band.

Keywords. reference systems, catalogs, astrometry, ICRF, interferometry, VLBI, radio continuum, Ka-band, galaxies: active galactic nuclei, quasars, blazars

1 Introduction

For over three decades now, radio frequency work in global astrometry, geodesy, and deep space navigation has been done at S-band (2.3 GHz) and X-band (8.4 GHz). While this work has been tremendously successful in producing 100 μas level global astrometry (*e.g.* Ma et al, 2009) and sub-cm geodesy, developments made over the last decade have made it possible to consider the merits of moving to a new set of frequencies. In this paper we present global astrometric results from X/Ka (8.4/32 GHz) observations.

Advantages: Moving the observing frequencies up by approximately a factor of four has several advantages. For our work in the Deep Space Network, the driver is the potential for higher data rates for telemetry signals to probes in deep space. Other advantages include 1) the spatial distribution of flux becomes significantly more compact (Charlot *et al*, 2010) lending hope that the positions will be more

stable over time, 2) Radio Frequency Interference (RFI) at S-band would be avoided, 3) Ionosphere and solar plasma effects on group delay and signal coherence are reduced by a factor of 15!

Disadvantages: While these are very significant advantages, they do not come without a price. The change from 2.3 / 8.4 GHz to 8.4 / 32 GHz moves one closer to the water vapor line at 22 GHz and thus increases the system temperature from a few Kelvins per atmospheric thickness up to 10–15 Kelvins per atmosphere or more. Thus one becomes much more sensitive to weather. Furthermore, the sources themselves are in general weaker and many sources are resolved. Also, with the observing wavelengths shortened by a factor of 4, the coherence times are shortened so that practical integration times are a few minutes or less—even in relatively dry climates. The shorter wavelengths also imply that the antenna pointing accuracy requirements must be tightened by the same factor of 4. The combined effect of these disadvantages is to lower the system sensitivity. Fortunately, advances in recent years in recording technology make it feasible and affordable to offset these losses in sensitivity by recording more bits. Thus while most of the X/Ka data presented in this paper used the same overall 112 Mbps bit rate as previous S/X work, recent data were taken at a 4 times higher rate with an increase to 8 times higher rate hoped for within the next year.

This paper is organized as follows: We will describe the observations, modelling, and present the results. Next, we will estimate the accuracy by comparing to the S/X-based ICRF2 (Ma et al, 2009) including a look at zonal errors. This will be complemented by a discussion of the error budget and the potential for improving the geometry of our network by adding a southern station.

2 The VLBI Observations

The results presented here are from fifty-one Very Long Baseline Interferometry (VLBI) observing sessions of ~ 24 hour duration done from July 2005 until April 2010 using NASA's Deep Space Stations

(DSS) 25 or 26 in Goldstone, California to either DSS 34 in Tidbinbilla, Australia or DSS 55 outside Madrid, Spain to form interferometric baselines of 10,500 and 8,400 km length, respectively. We recorded VLBI data simultaneously at X-band (8.4 GHz) and Ka-band (32 GHz). Initially, sampling of each band was at 56 Mbps while more recent passes used 160/288 Mbps at X/Ka. Each band used a spanned a bandwidth of ~ 360 MHz. The data were filtered, sampled, and recorded to the Mark4 or Mark5A VLBI systems. The data were then correlated with the JPL BlockII correlator (O'Connor, 1987) or the JPL SOFTC software correlator (Lowe, 2005). Fringe fitting was done with the FIT fringe fitting software (Lowe, 1992). This procedure resulted in 12,860 pairs of group delay and phase rate measurements covering the full 24 hours of right ascension and declinations down to -45 deg. Individual observations were about 1 to 2 minutes in duration.

3 Modelling

The above described set of observations were then modelled using the MODEST software (Sovers, Fanselow, & Jacobs, 1998). A priori Earth orientation was fixed to the MHB nutation model (Mathews *et al*, 2002) and the empirically determined UT1-UTC and Polar Motion of the Space 2008 series (Ratcliff & Gross, 2010). The celestial frame was aligned to the ICRF2 defining sources (Ma *et al*, 2009) using a No-Net-Rotation constraint (Jacobs *et al* 2010). Station velocities were estimated; station locations were estimated with a 1 cm constraint per component to a decades-long S/X-band VLBI solution.

4 Results

In all, we detected 436 extragalactic radio sources which covered the full 24 hours of RA and Declinations down to -45 deg. In Fig. 1 these sources are plotted using an Aitoff projection to show their locations on the sky. RA= 0 is at the center. The ecliptic plane is shown by the dashed blue-gray line and the Galactic plane is indicated by the yellow-red dashed line. The sources are color coded according to their 1-sigma formal declination uncertainties with the value ranges indicated in the figure's legend. Note that the declination precision drops as one moves toward the south. This is a result of having significantly less data on the California to Australia baseline combined with the need to observe sources closer to the horizon as declination moves south thus incurring greater error from higher system temperatures and tropospheric mis-modelling.

5 Accuracy: X/Ka vs. S/X comparisons

Experience shows that formal uncertainties tend to underestimate true errors. An independent estimate of the position errors was obtained by comparing our X/Ka-band positions to the S/X-based ICRF2. For 372 common sources, the differences in the sense X/Ka minus S/X are shown for $\Delta\alpha \cos \delta$ in Fig. 2 and for $\Delta\delta$ in Fig. 3. Weighted RMS (wRMS) differences are $\sim 200 \mu\text{as}$ in $\alpha \cos \delta$ and $\sim 290 \mu\text{as}$ in δ .

6 Zonal Errors

In astrometry it is easier to measure the relative positions of nearby sources than to accurately measure sources that are separated by long arcs. Fig. 4 shows the mean arclength difference vs. arclength in the sense (X/Ka - S/X). As expected, arclengths agree better for short arcs and gradually worsen as arcs grow longer out to a mean differences of $\sim 100 \mu\text{as}$ at arcs of ~ 70 to 130 deg. The peak difference occurs at that separation due to declination differences. Arcs longer than ~ 130 degrees must be more in the RA direction which is less effected by systematic errors. Hence, the arc differences decrease for the longest arcs.

7 Discussion of Error Budget

Having assessed the size of errors in our positions using the much larger ICRF2 S/X data set as a standard of accuracy, we now discuss the major contributions to the errors in the X/Ka measurements: SNR, instrumentation, and troposphere. Fig. 5 shows the weighted RMS group delay vs. the Ka-band SNR. We conclude that for SNR < 15 dB, the thermal error dominates the error budget. For higher SNRs, troposphere and instrumentation errors become important. Binning of wRMS delay vs. airmass thickness shows that troposphere is not the dominant error due to the generally low SNRs just mentioned. However, the phase rates (which carry much less weight in the fit) are dominated by errors from tropospheric mis-modelling, thus hinting that troposphere will become more important as our SNR improves with increased data rates. Lastly, we have errors from un-calibrated instrumentation. A proto-type phase calibrator was developed in order to calibrate the signal path from the feed to the sampler (Hammel *et al*, 2003). Test data shown in Fig. 6 indicate an approximately diurnal instrumental effect with ~ 180 psec (~ 6 cm or ~ 6 nrad or $\sim 1200 \mu\text{as}$) RMS. Although the data themselves can be used to estimate instrumental parameters which partially characterize this effect, operational phase calibrators are being built in order to

achieve accuracy of better than 1 part-per-billion (1 nrad, 200 μ as) in a timely fashion.

8 Southern Geometry

Besides the three classes of measurement errors described above, our reference frame suffers from a very limited geometry—we have only one station in the southern hemisphere. In order to better understand this limitation, we simulated the effect of adding a second southern station (Bourda, Charlot, & Jacobs, 2010). Data from 50 real X/Ka sessions (Fig. 7) were augmented by simulated data (Fig. 8) for 1000 group delays each with SNR = 50 on a \sim 9000 km baseline: Australia to S. America or S. Africa. The resulting solution extended Declination coverage to the south polar cap region: -45 to -90 deg. Precision in the south cap region was \sim 200 μ as (1 nrad) and in the mid south precision was 200–1000 μ as, all with just a few days observing. We conclude that adding a second southern station would greatly aid our X/Ka frame’s accuracy. In fact, the resulting four station network should compete well in astrometric accuracy with the historical S/X network and its ICRF2.

9 Conclusion

The S/X-based ICRF has now been extended to four times higher frequency to X/Ka-band (8.4/32 GHz). A total of 436 sources have been successfully detected at Ka-band. For the 372 sources common to X/Ka and the S/X-based ICRF2, we find positional agreement of 200 μ as (1 nrad) in $\alpha \cos \delta$ and 290 μ as (1.4 nrad) in δ with zonal errors of \sim 100 μ as (0.5 nrad). Improvements in data rates and instrumental calibration are projected to allow better than 200 μ as (1 nrad) accuracy within the next few years. Simulations of adding another southern station predict better than 200 μ as accuracy for the southern polar cap within a very short time of adding data from an all southern baseline. This gives hope that better than 100 μ as accuracy over the full sky might be achieved within a few years of adding a southern baseline.

10 Acknowledgements

The research described herein was performed at the Jet Propulsion Laboratory of the California Institute of Technology, under a contract with the National Aeronautics and Space Administration. Government sponsorship acknowledged. Copyright 2011 ©. All rights reserved.

References

- Bourda, G., P. Charlot, and C.S. Jacobs, (2010) ‘Future Radio Reference Frames and Implications for the Gaia Link,’ Proc. of ELSA Conference: Gaia at the Frontiers of Astrometry, Sevres, France.
ftp.hip.obspm.fr/gaia2010/IMG/pdf/Poster_Bourda.pdf
- Charlot, P., D.A. Boboltz, A.L. Fey, E.B. Fomalont, B.J. Geldzahler, D. Gordon, C.S. Jacobs, G.E. Lanyi, C. Ma, C.J. Naudet, J.D. Romney, O.J. Sovers, and L. D. Zhang, (2010), ‘The Celestial Reference Frame at 24 and 43 GHz II. Imaging, AJ, 139, 5, 1713,
<http://iopscience.iop.org/1538-3881/139/5/1713/>
doi: 10.1088/0004-6256/139/5/1713
- Hamell, R., B. Tucker, & M. Calhoun, (2003), ‘Phase Calibration Generator,’ NASA JPL IPN Prog. Report, 42-154, pp. 1–14, 15 Aug.,
tmo.jpl.nasa.gov/progress_report/42-154/154H.pdf
- Jacobs, C.S., M.B. Heflin, O.J. Sovers, and J.A. Steppe, (2010), ‘CRF Rotational Alignment Significantly Altered by RA-Dec Correlations,’ IVS 2010 Gen. Meeting Proc., eds. D. Behrend & K. D. Baver, NASA/CP-2010-IVS Analysis Session, Hobart, Tasmania, Australia.
[ftp://ivsc.gsfc.nasa.gov/pub/general-meeting/2010/presentations/GM2010_AW_jacobs.pdf](http://ivsc.gsfc.nasa.gov/pub/general-meeting/2010/presentations/GM2010_AW_jacobs.pdf)
- Lowe, S.T., (1992) *Theory of Post-BlockII VLBI Observable Extraction*, JPL Pub. 92-7, Pasadena CA,
ntrs.nasa.gov/archive/nasa/casi.ntrs.nasa.gov/19940009399_1994009399.pdf
- Lowe, S. T., (2005) *SOFTC: A Software VLBI Correlator*, JPL section 335 internal document, Jet Propulsion Laboratory, Pasadena, CA.
- Ma, C., E.F. Arias, T.M. Eubanks, A.L. Fey, A.-M. Gontier, C.S. Jacobs, O.J. Sovers, B.A. Archinal, and P. Charlot, (1998), ‘The ICRF as Realized by VLBI,’ AJ, 116, 1, 516–546.
iopscience.iop.org/1538-3881/116/1/516/
doi: 10.1086/300408
- Ma, C., *et al.*, (2009), editors: A.L. Fey, D. Gordon & C.S. Jacobs, IERS Tech Note 35: ‘The 2nd Realization of the ICRF by VLBI,’ IERS, Frankfurt, Germany, Oct. 2009.
http://www.iers.org/nn_11216/IERS/EN/Publications/TechnicalNotes/tn35.html
- Mathews, P. M., T. A. Herring, and B. A. Buffet, (2002), ‘Modeling of Nutation and Precession: New nutation series for Nonrigid Earth and Insights into the Earth’s Interior,’ JGR, 107, B4, 10.1029/2001JB000390.
www.agu.org/journals/jb/jb0204/2001JB000390/
- O’Connor, T., (1987) *Introduction to the BlockII Correlator hardware*, JPL internal publication, Pasadena CA.
- Ratcliff, J.T., and R.S. Gross, (2010), *Combinations of Earth Orientation Measurements: Space 2008, COMB2008, and POLE 2008*, JPL Publication 10-4, Pasadena CA. <http://hdl.handle.net/2014/41512>
- Sovers, O.J., J.L. Fanselow, & C.S. Jacobs, (1998), ‘Astrometry, Geodesy with Radio Interferometry: Expts., Models, Results,’ Rev. Mod. Phys., 70, 4, 1393–1454.
link.aps.org/doi/10.1103/RevModPhys.70.1393
doi: 10.1103/RevModPhys.70.1393

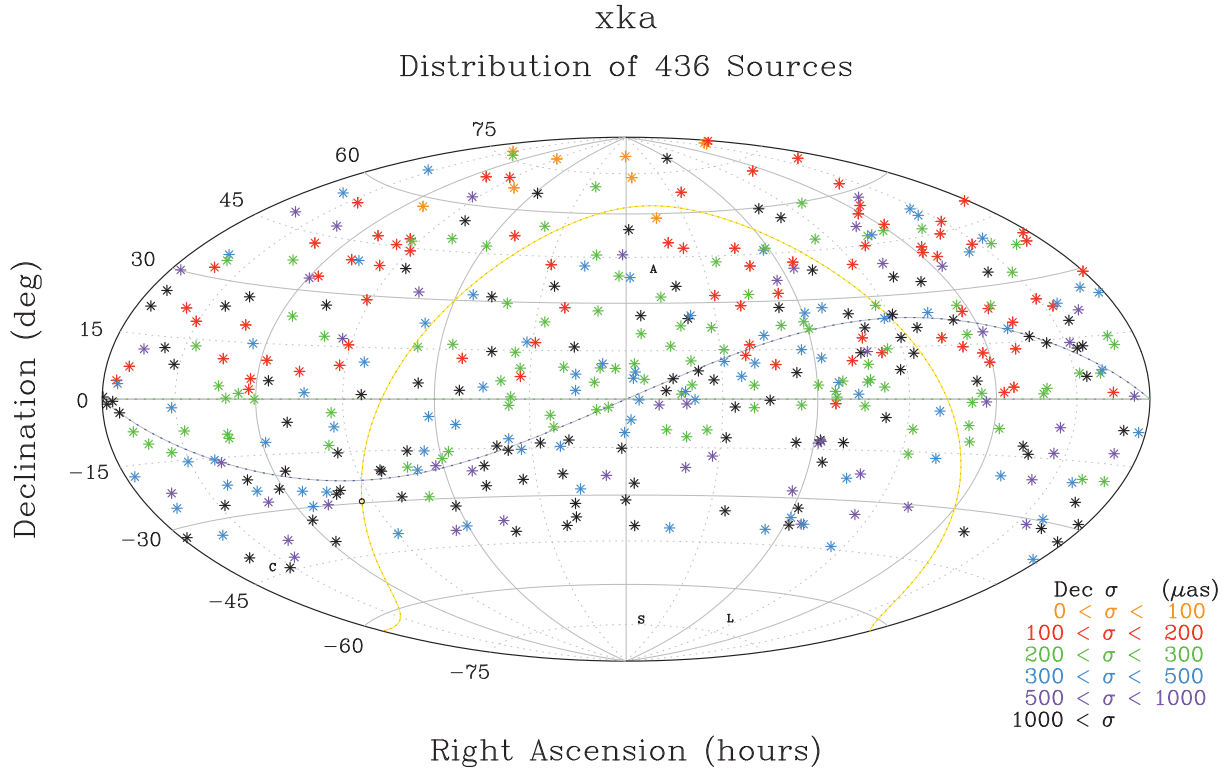


Figure 1. Distribution of 436 X/Ka-band sources detected to date. Symbols indicate $1\text{-}\sigma$ formal declination uncertainties as defined in the legend at lower right. $(\alpha, \delta) = (0, 0)$ is at the center. The ecliptic plane is indicated by a dashed line. The galactic plane is indicated by the Ω -shaped line. Note the trend for decreasing declination precision moving southward. Local galactic neighborhood indicated by A, C, S, L: Andromeda, Centaurus-A, Small & Large Magellanic clouds (none observed at X/Ka).

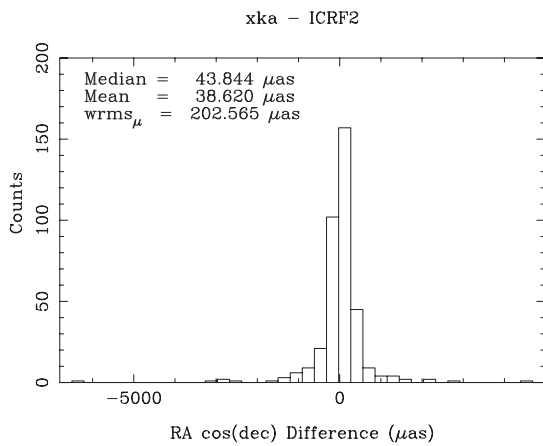


Figure 2. X/Ka - S/X: $\Delta\alpha \cos \delta$

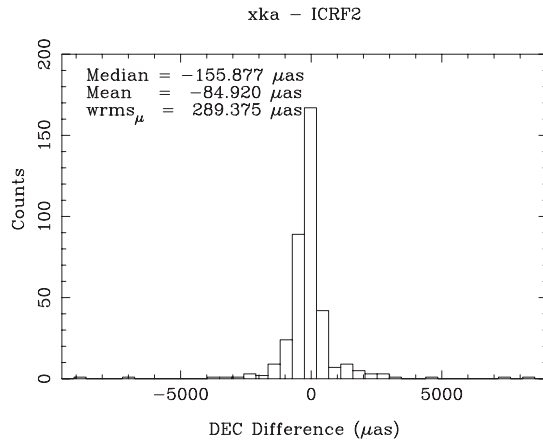


Figure 3. X/Ka - S/X: $\Delta\delta$

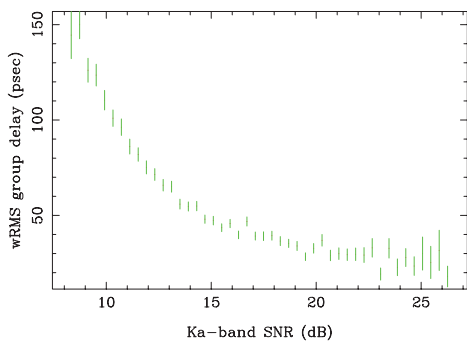


Figure 4. The wRMS residual group delay vs. Ka-band SNR. Thermal error dominates the VLBI residuals for SNR < 15 dB. As SNR increases past that point, a noise floor of ≈ 30 psec from tropospheric and instrumental errors is asymptotically approached.

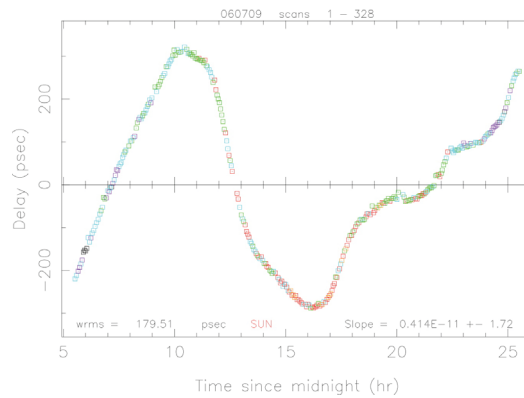


Figure 5. Ka-band proto-type phase calibrator group delays vs. time from 9 Jul 2006. Diurnal variation is driven by thermal changes in cables and other instrumentation. Color code indicates the sun angle (in order closest to farthest: orange, red, green, cyan, purple, black).

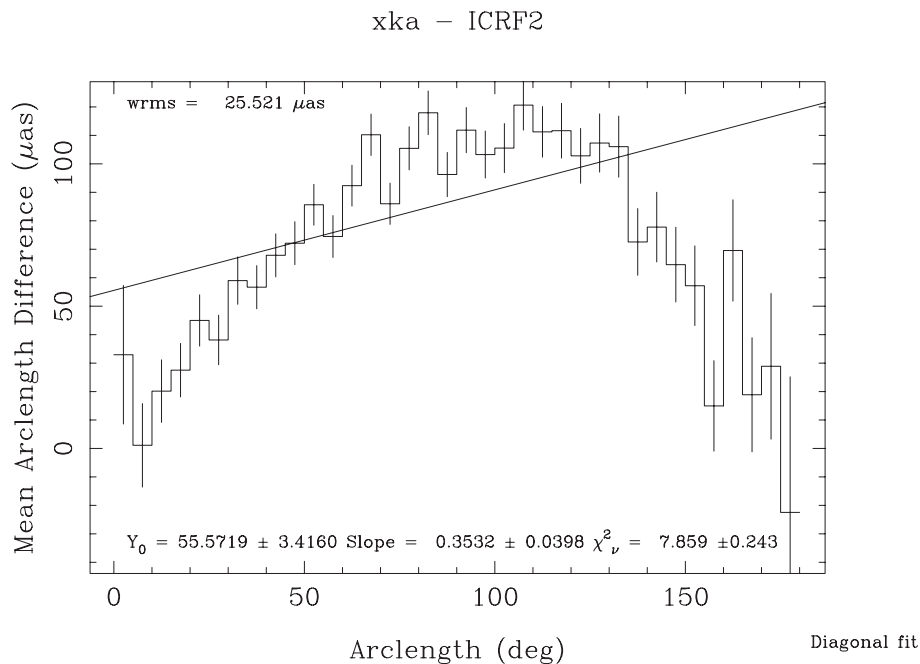


Figure 6. Zonal errors: Mean arc differences vs. arc length for X/Ka – S/X(ICRF2)

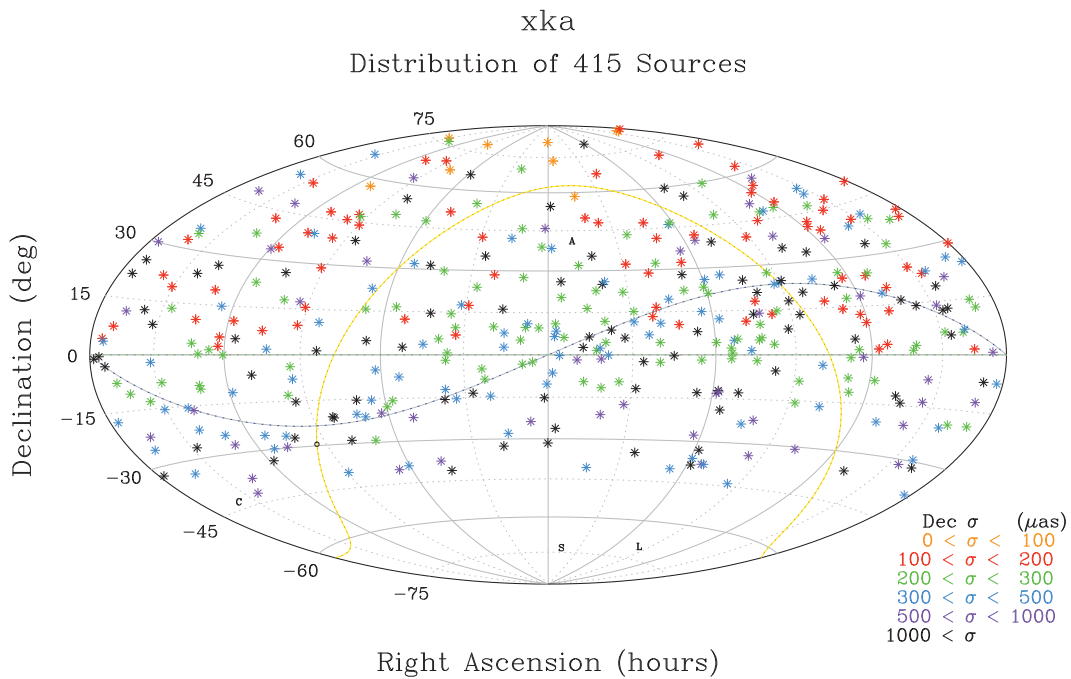


Figure 7. Real X/Ka data from 50 sessions using two baselines: CA-Spain and CA-Australia

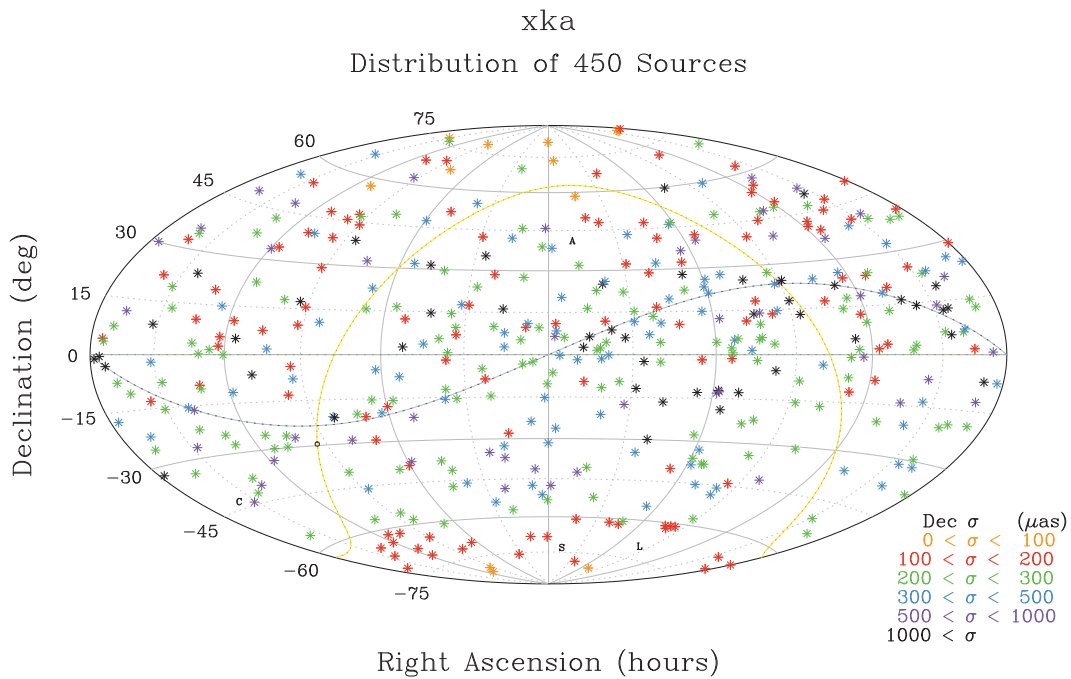


Figure 8. After adding 1000 delays from a simulated 3rd baseline in the south, the southern cap would be covered with sources of $\sim 200 \mu\text{as}$ precision (color code same as Fig. 1).